Molecular Dynamics Simulations of the Interior of Aqueous Reverse Micelles

J. Faeder and B. M. Ladanyi*

Department of Chemistry, Colorado State University, Ft. Collins, Colorado 80523

Received: August 30, 1999; In Final Form: November 11, 1999

Aqueous reverse micelles, which are surfactant aggregates in nonpolar solvents that enclose packets of aqueous solution, have been widely studied experimentally and theoretically, but much remains unknown about the properties of water in the interior. The few previous molecular dynamics simulations of reverse micelles have not examined how the micelle size affects these properties. We have modeled the interior of an aqueous reverse micelle as a rigid spherical cavity, treating only the surfactant headgroups and water at a molecular level. Interactions between the interior molecules and the cavity are represented by a simple continuum potential. The basic parameters of the model—micelle size, surface ion density, and water content—are based on experimental measurements of Aerosol OT reverse micelles but could be chosen to match other surfactant systems as well. The surfactant head is modeled as a pair of atomic ions: a large headgroup ion fixed at the cavity surface and a mobile counterion. The SPC/E model is used for water. The simulations indicate that water near the cavity interface is immobilized by the high ion concentration. Three structural regions of water can be identified: water trapped in the ionic layer, water bound to the ionic layer, and water in the bulklike core. The basic properties of bulk water reemerge within a few molecular layers. Both the structure and dynamics of water near the interface vary with micelle size because of the changing surface ion density. The mobility of water in the interfacial layers is greatly restricted for both translational and rotational motions, in agreement with a wide range of experiments.

1. Introduction

In nonpolar solutions certain amphiphilic molecules form aggregates with their polar headgroups on the interior, leading to their description as "reverse micelles".[1-8] When a small amount of polar solvent—most commonly water—is added, the micelles swell, creating a new, confined liquid phase on the inside. Figure 1 shows a common surfactant molecule and illustrates the basic structure of an aqueous reverse micelle. Experimental studies of these structures with a range of techniques have shown that they consist of tens to hundreds of surfactant and solvent molecules and tend to be spherical in shape at low surfactant and polar solvent concentrations.[9-14] The effects of confinement and the strong interactions between the polar solvent molecules and the headgroups, which are frequently ionic, produce a chemical environment that may differ dramatically from that of the bulk solvent. As more polar solvent is added, the interior pools grow in size and tend to recover the properties of the bulk solvent. Some authors use the term "microemulsion" to distinguish these larger aggregates with a more bulklike interior from the smaller ones,[12,15] but we use the description "reverse micelles" to refer to all spherical aggregates occurring in predominantly nonpolar surfactant mixtures.

The properties of this interior phase and their variation with micelle size are interesting for both fundamental and practical reasons. In biochemistry, reverse micelles have been widely studied because of their resemblance to biological membranes, and they have also been exploited for their ability to solubilize enzymes and catalyze biochemical reactions.[16] Reverse micelles have been applied to chemical catalysis, drug delivery, nano-
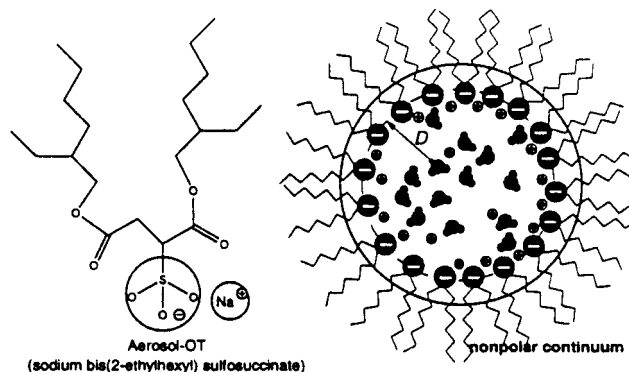

Figure 1. Structure of Aerosol OT and the interior of a spherical, aqueous reverse micelle.

cluster synthesis, and materials development,[2,5,6,16-18] and they have frequently been described as "microbeakers" or "microreactors".

A major reason that reverse micelles are so useful for chemistry is that they create a large interface between the aqueous and nonpolar phases, allowing reactants that prefer different phases to be brought together. For example, most enzymes, being highly polar molecules, are much more soluble in aqueous phases, but many substrates are soluble only in nonpolar solutions, so that reactions between the two will only occur if there is a sufficient interface between the phases. Because much chemistry occurs at the reverse micellar interface, it is important to understand the properties of the solvent there. From both experimental[19-24] and theoretical[25-36] studies of water at many different types of interfaces, it is known that most of the changes occur over a range of only a few molecular diameters, and properties of the bulk reemerge rapidly at greater

distances. It is therefore important to characterize the solvent interfacial structure at a molecular level.

The size of reverse micelles ranges from a few solvent molecule diameters to many hundreds.[5,6] The overall size of the cavity is obviously an important factor in micellar reactivity, controlling such factors as reactant concentrations, the position of reactants within the cavity, and the size of product particles.[16,18] Sometimes less appreciated are the changes in interfacial properties that occur as the reverse micelle size is varied. Curvature is one important property,[37-39] but probably more important for reactivity are the changes in the concentrations of the polar surfactant groups at the interface, which have a large effect on the structure of both the surfactant layer and the interfacial solvent. One fundamental motivation for studying reverse micelles is that they provide a well-controlled system for observing the effects of charge variation at an interface, a problem of broad interest to chemistry and biology.

One the most commonly studied surfactants that forms reverse micelles is sodium bis(2-ethylhexyl)sulfosuccinate, also known as Aerosol OT (AOT).[5] Because of its two branched hydrocarbon chains (see Figure 1), this molecule possesses a high ratio of hydrophobic tail volume to headgroup surface area, which is predicted by basic thermodynamic models to be a key factor in reverse micelle formation.[40] AOT is attractive as a model surfactant because it does not require cosurfactants to form reverse micelles. Aqueous AOT reverse micelles can be characterized over a wide range of water and surfactant concentrations by a single parameter,

$$w_0 = [H_2O]/[AOT] \tag{1}$$

which is proportional to the micellar radius.[12,13] These aggregates have been found to be relatively monodisperse in solution and spherical in shape down to very low water concentrations.[14] The spherical aggregates, which are the focus of this study, range in the diameter of the aqueous core from about 0.5 nm to more than 10.0 nm.

The vast number of experimental studies and applications of AOT reverse micelles have recently been reviewed by De and Maitra.[5] Experimental techniques that have been used to characterize the AOT reverse micelles include light scattering,[41,42] photon correlation,[12] IR spectroscopy,[23,43-47] NMR,[11,22,48-52] probe fluorescence,[10,21,53-61] calorimetry,[62,63] small-angle neutron scattering (SANS),[13,14,64] and quasi-elastic neutron scattering.[65,66] While many of these techniques provide information about the structure and properties of reverse micelles, a fundamental dispute remains about the structure of water in the micellar interior. A large number of investigators (the majority of those cited) have fit their data by assuming that water adopts two or more distinct structures in the interior. The simplest models postulate two different water structures, "bound" and "free", corresponding to water that is bound to the headgroup ions at the interface and water that has more bulklike characteristics away from the interface. Bound water in these models has, in comparison to bulk water, greatly restricted mobility— both translational[65,66] and rotational,[11,22,32,48,49] increased viscosity,[21] a diminished hydrogen-bonding network,[23,43-47] and less polarity[10,11] or smaller dielectric constant.[53] The transition from the highly rigid behavior of the smallest reverse micelles to the more fluid properties that approach the bulk in the largest reverse micelles has often been modeled by a decrease in the ratio of bound to free water molecules. There is, however, no direct experimental characterization of the molecular water structure at the interface, and other researchers have suggested that water has a uniform structure within the interior,[43,52,67] which is

affected only by the overall ion concentration and not by local effects. They argue that previous experiments that were modeled by multistate models, where each state has fixed properties as a function of micelle size, can also be modeled by a single state whose properties vary with size.

Recently, several groups have used time-resolved fluorescence to characterize the solvation response in reverse micelles on the nanosecond,[54] picosecond,[55-57] and femtosecond time scales.[59,60,68] They have found that substantial components of the response occur on time scales several orders of magnitude longer than those found in bulk water and even concentrated electrolyte solutions.[68] It is thought that significant portions of this response are due to the highly restricted mobility of water, particularly bound water, inside the reverse micelles. In addition, even the short-time components of the solvation response appear to be longer compared with the bulk.[59,60,68] Ultrafast terahertz spectroscopy has also been used to probe the dielectric relaxation of water in AOT reverse micelles,[69] and it was found that both the magnitude and time scale of the response were smaller than those in bulk water. The increase in the frequency of the dielectric response in the terahertz experiments seems to conflict with the much longer relaxation times found in the fluorescence experiments. Nevertheless, these experiments suggest that the restricted mobility of water inside reverse micelles can have a large effect on the collective properties of the solvent. The uncertainty surrounding the structure of water in these environments, however, hinders the interpretation of the results.

In this paper we investigate the properties of a simple molecular model for the interior of an aqueous reverse micelle with the aim of elucidating the structure and dynamics of water in these environments. In this model, the surfactant tails and surrounding nonpolar solvent are treated as a continuum, and the interior is described by a rigid spherical cavity containing surfactant headgroup ions tethered to the cavity, mobile counterions, and water molecules. The sizes of the ions are chosen to match those of the sulfonate and sodium in AOT and the compositions of the model micelles as determined from the experimental aggregation numbers.[41] Simulations have been performed over a range of micelle sizes of $1 \leq w_0 \leq 10$. The results of the simulations show that for all of the sizes studied water forms distinct molecular layers, which are easily observed in water density profiles. We have characterized the structural and dyanamical properties of these layers using a variety of other measures described below and compared our results to both experimental observations and other simulations. The remainder of the paper is organized as follows: Section 2 discusses previous molecular modeling of reverse micelles, section 3 presents the current model, section 4 contains a detailed analysis of simulation results, section 5 compares these results with those of other simulations and experiments, and section 6 concludes.

2. Previous Molecular Modeling of Reverse Micelles

Molecular modeling of these complex systems is a daunting task. The few previous molecular simulations of reverse micelles have been of two basic types: (1) atomistic models that include nonpolar solvent, surfactant, and polar solvent molecules (and possibly additional aqueous solutes) explicitly and (2) reduced models that use simplified potentials to treat the interactions of the polar molecules on the interior with the nonpolar components on the exterior. All of the molecular models to date, including the one presented here, neglect intermicellar interactions.

Atomistic models offer the potential for a complete description of the molecular structure in these systems, but the

simulations are cumbersome and expensive, while with reduced models it is easier to study the effect of the fundamental parameters, such as micelle size, counterion charge and size, and temperature. To date, however, no one has to our knowledge studied in a systematic way the properties of even simplified molecular models of reverse micelles. Of the three atomistic simulations of a complete reverse micelle, two simulate micelles with an effectively solid core consisting largely of calcium carbonate.[70,71] Alaimo and Kumosinski[72] have simulated a complete AOT reverse micelle using an all-atom potential, but they examined only the issue of aggregrate stability. Derecskei et al.[73] have performed all-atom simulations of a single AOT molecule with solvent shells of water and carbon tetrachloride. In the future their simulations may be extended to include a complete reverse micelle, and it will be interesting to compare the all-atom description with the results obtained here.

Brown and Clarke[74] carried out what, to our knowledge, was the first molecular dynamics (MD) simulation of a reverse micelle by using simplified, single-site interaction models for the nonpolar solvent molecules, hydrocarbon tails, and head-groups. They showed that their carefully assembled model micelle was mechanically stable on the time scale of the simulation (100 ps) and investigated the shape fluctuations and structural properties of the water and ions. The headgroups in this model were, however, positively charged ions much smaller than the sulfonate headgroups of AOT. Furthermore, the mobile counterions were negatively charged and substantially larger than the Na^+ ions in AOT. Most important is that only a single, relatively small, micelle was studied, so the effect of micelle size on the structure could not be assessed.

Linse and Halle[32,50] also performed MD simulations with an even more simplified model, which included discrete representation of only the headgroups, counterions, and water molecules. The headgroups were embedded in the surface of a hollow cavity, and the interaction between the hydrophobic cavity exterior and the water molecules and the counterions on the interior was represented by a single potential, the spherical equivalent of the 3−9 potential commonly used for the interaction between molecule and a hydrophobic surface.[26,75] Linse conducted a detailed structural analysis of this system,[32] but only a single size was studied, and the surface ion coverage that was chosen (90 Å^2) is about a factor of 2 smaller than what is found in equivalent AOT reverse micelles. The ionic charges were also scaled so that the total strength of the ionic interactions was about 50% smaller than that in the system with full charges.

3. Methods

The model used in the current simulations is similar to the one used by Linse and Halle, but it has been modified to provide a more realistic representation of AOT reverse micelles. An illustration of the model is shown in Figure 2. The micelle exterior is still represented by a continuum potential, but the headgroups, rather than being embedded in the cavity, protrude from the interface as might be expected from the structure of the AOT molecule (see Figure 1). Other differences, including the headgroup and water models, are detailed below. Another key difference between the two models is that experimental aggregation numbers have been used to determine the parameters that define the model system for a given value of w_0. Thus, the density of ions at the micelle interface, a key factor in determining the molecular structure of the interface should be approximately correct. While the incorporation of experimental data should make this model more realistic for AOT reverse micelles than previous models, it still contains several
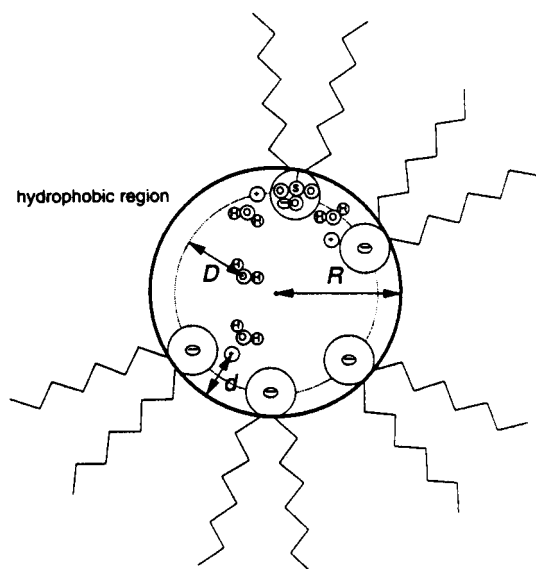

Figure 2. Model of the reverse micelle interior. The solid circle marks the boundary of the hydrophobic cavity. The sulfonate headgroups are modeled as a single atomic ion with a charge of −e. The dotted circle shows the equilibrium positions of the headgroups, which are confined by a harmonic potential, and also marks the van der Waals radius of the cavity. D marks the distance between an atomic center and the dotted circle, while d is the distance to the cavity boundary. R is the total radius of the cavity.

simplifications— the rigid spherical shape of the interface, the lack of penetration by water into the hydrophobic region, the spherical description of the headgroup anion, and the absence of surface roughness— all of which are known to be violated to some degree in the experimental system. The effect of these and other approximations will be addressed in future work.

3.1. Potential Model. We have modeled the interior of an aqueous reverse micelle as a rigid spherical cavity, treating only the surfactant headgroups and water at a molecular level. Interactions between the interior molecules and the cavity are represented by the same continuum potential used by Linse and Halle,[50] described in more detail below. The surfactant head-group is modeled as a pair of atomic ions: a large negative ion fixed at the cavity interface approximates the sulfonate group, while a much smaller positive ion represents Na^+. Interactions between different reverse micelles are neglected in the model, corresponding to the condition of infinite dilution. As a result, periodic boundary conditions are not required.

The interaction potentials among the various components of the system are handled in the standard way as a sum of Lennard-Jones and point charge interactions. The positive and negative ions are each assigned a unit charge, while the SPC/E model[76] is used for both the charge distribution and Lennard-Jones interactions of water. This rigid water model has been extensively used in liquid simulations and gives reasonable values for a wide range of both water[77−79] and ion−water properties.[80] The size of the large atomic ion (Z^-) representing sulfonate was determined by adding the S−O bond length to the approximate van der Waals radius of the sulfonate O atom, resulting in a total value for σ_{Z^-} of 6 Å. The value of ϵ_{Z^-}, which is of minimal importance in this system, was assigned the reasonable value of 0.5 kcal/mol. The parameters for Na^+ were taken from a previous simulation involving water and sodium dodecyl sulfate.[81] For convenience, all of the potential parameters used in the model are shown in Table 1. The Lennard-Jones parameters for interactions between sites of different type

TABLE 1: Potential Model Parameters[a]

atom	σ (Å)	ϵ (K)	q (e)
O	3.166	78.24	-0.8476
H			0.4238
Z^-	6.0	251.58	-1.0
Na^+	2.275	58.01	1.0

[a] $R_{O-H} = 1$ Å; $\angle_{HOH} = 109.5°$. $\sigma_{wall} = 2.5$ Å; $\epsilon_{wall} = 231.55$ K. $d_e = 2.5$ Å; $k_e = 600$ kcal/mol Å^{-2}.

are determined from the usual combining rules

$$\sigma_{ij} = (\sigma_i + \sigma_j)/2, \qquad \epsilon_{ij} = (\epsilon_i\epsilon_j)^{1/2} \qquad (2)$$

Although these effective pair potentials do not accurately treat many-body interactions, more complicated potentials that explicitly include many-body polarization have given only slightly different results at similar interfaces for the simple structural and dynamical properties examined in this paper.[82]

The interaction potential between the cavity and a site on the interior is determined by assuming the cavity is composed of a continuum of sites at constant density, where the interaction between the interior and exterior sites is given by a Lennard-Jones potential. Integrating over all points on the cavity exterior gives the interaction energy[50]

$$u(z \equiv r/R) = 8\pi\rho_{hc}\epsilon\sigma^3[(\sigma/R)^9 F(z,6) - (\sigma/R)^3 F(z,3)] \quad (3)$$

where

$$F(z,n) = \int_1^\infty y^2 \, dy \int_{-1}^1 \frac{dx}{(y^2 + z^2 - 2xyz)^n} \qquad (4)$$

R is the total radius of the cavity, r is the distance of the site from the cavity center, and ρ_{hc} is the density of sites in the hydrocarbon exterior. The functions $F(z,3)$ and $F(z,6)$ are given by

$$F(z,3) = 2/[3(1 - z^2)^3]$$

$$F(z,6) = 2(5 + 45z^2 + 63z^4 + 15z^6)/[45(1 - z^2)^9] \quad (5)$$

It can be shown that in the limit of infinite R (zero curvature) this potential, when expressed as a function of the distance from the interface, d, attains the standard 3−9 form that has been commonly used for the interaction of a particle and a flat hydrophobic surface. In terms of the parameters previously used to specify this interaction, σ_{wall} and ϵ_{wall}, the sphere potential becomes

$$u(z) = $$
$$18\sqrt{3}\epsilon_{wall}[(15/2)(\sigma_{wall}/R)^9 F(z,6) - (\sigma_{wall}/R)^3 F(z,3)] \quad (6)$$

so that in the limit of zero curvature σ_{wall} and ϵ_{wall} mark the zero crossing and the minimum of the potential, respectively. Only the sodium and oxygen atoms interact with the cavity through this potential. The values of σ_{wall} and ϵ_{wall} (see Table 1) are the same for both atom types and are taken from ref 26.

The structure of the cavity interface in the current model differs from that of Linse and Halle,[50] in which the headgroup ions were embedded in the cavity interface. As shown in Figure 2, the Z^- ions protrude from the cavity by a distance of 2.5 Å, a difference that must be considered when calculating the effective ion densities at the surface that are shown in Table 2. The Z^- ions are held at the interface by a harmonic potential of the form

$$u(d) = (1/2)k_e(d - d_e)^2 \qquad (7)$$

where k_e has the value 600 kcal/mol Å^{-2}, which is roughly appropriate for a covalent bond.[81] The Z^- ions may move freely on the surface of the interface but are effectively prevented from doing so by their strong repulsion for each other. The protrusion of the Z^- ions from the surface, which is strongly suggested by the structure of AOT, allows both the counterions and water molecules to occupy bridging positions directly between the negative ions and thus lowers the interaction energy at the interface.

3.2. Construction of the Reverse Micelles. The three fundamental parameters used to define our model system are the number of surfactant molecules, n_s, the ratio of water molecules to surfactant molecules, w_0, and the micelle radius, R. For a given value of w_0, n_s has been determined by linear interpolation of Eicke and Rehak's reported values of $\langle n_s \rangle$ measured in the water/AOT/isooctane system by light scattering.[41] The total volume of the system, V, can then be calculated by assuming a fixed molecular volume for each of the three species in the micelle. The molecular volume of water was assumed to be the bulk value of 30 Å^3 (0.997 g/cm^3), based on the density of water at 25° C, while the molecular volumes of Na^+ and Z^- were taken to be 6 and 57 Å^3, respectively. The latter values are the spherical volume ($\pi\sigma^3/6$) of Na^+ and half this volume for Z^-. R is then given by $(3V/4\pi)^{1/3} + \sigma_{wall}$. This determination of R is obviously approximate, but we have found that the structural properties do not depend sensitively on R. Supporting the validity of this procedure is the fact that the water density in the core approaches that of the bulk in the larger micelles. The parameter sets used in the current simulations are shown in Table 2.

The reverse micelles were constructed in a three-step process. First, the Z^- ions were distributed on a sphere of radius $R - d_e$, and the repulsive interactions were minimized by geometry optimization with the ions constrained to lie on the surface of the sphere. Then, with the negative ions held fixed, the counterions were randomly distributed inside the cavity, and the lowest energy configuration was determined from a series of Monte Carlo heating and annealing cycles, after which the counterions all lay at the interface and were bound to one or more headgroup ions. The water molecules were then added to the cavity, the constraints on the negative ions were removed, and the system was allowed to equilibrate at 500 K by running an MD trajectory for several hundred picoseconds, after which the temperature was lowered to 300 K over an additional 100−200 ps. The trajectory was continued for another 50−200 ps to equilibrate the system at 300 K.

We have tested several modifications of this procedure and found that the results are not sensitive to how the micelle is constructed, provided sufficient time is allowed for equilibration. The structural properties of the reverse micelles do, however, vary from run to run. Different structural isomers appear to form during the annealing process that do not interconvert at 300 K on time scales of up to several nanoseconds. The variations in the properties of these distinct structures are small enough that they generally do not affect the observed trends with micelle size.

3.3. Simulations. Integration of the MD trajectories was performed using the velocity Verlet algorithm with the method of constraints to maintain the rigidity of the water molecules.[83,84] A 2 fs step size was used throughout the simulations. The temperature was controlled using the Berendsen thermostat[85] with a time constant of 0.4 ps during the equilibration period

TABLE 2: Overview of the Simulations

run[a]	w_0	n_s	n_{H_2O}	R (Å)	f^b (Å²)	run time (ns)	$\langle PE_{tot} \rangle^c$ (10^3 kJ/mol)	$\langle PE_{H_2O} \rangle$ (kJ/mol)	$\langle$ pressure $\rangle$ (bar)
RM1a	1.0	21	21	10.25	35.9	2.0	−12.555(3)	−78.9	$7.2(2) \times 10^3$
RM1b	1.0	21	21	10.25	35.9	2.0	−12.594(3)	−80.9	$6.8(2) \times 10^3$
RM2a	2.0	26	52	11.6	40.0	2.0	−17.101(3)	−75.1	$3.4(1) \times 10^3$
RM2b	2.0	26	52	11.6	40.0	2.0	−17.072(3)	−88.8	$3.3(1) \times 10^3$
RM3	3.0	32	96	13.15	44.5	0.5	−22.699(3)	−73.9	$1.1(1) \times 10^3$
RM4a	4.0	35	140	14.1	48.3	0.5	−26.651(3)	−76.4	$6.2(6) \times 10^2$
RM4b	4.0	35	140	14.1	48.3	0.5	−26.672(5)	−77.1	$4.4(7) \times 10^2$
RM7.5	7.5	70	525	19.4	51.3	1.0	−65.613(2)	−70.4	$0.4(2) \times 10^2$
RM10	10.0	98	980	22.9	53.4	0.4	−103.60(2)	−68.6	$−1.3(1) \times 10^2$
HC174		0	174	13.4		0.5	−7.437(3)	−42.7	$2.4(3) \times 10^1$
HC674		0	674	19.4		0.5	−29.831(5)	−44.2	$4.6(3) \times 10^1$
B216		0	216			0.1	−10.065(5)	−46.6	$3(3) \times 10^1$

[a] RM, HC, and B refer to reverse micelle, hydrophobic cavity, and bulk, respectively. [b] $f = 4\pi(R - d_e)^2/n_s$ is the area occupied per surfactant molecule at the interface. [c] $\langle PE_{tot} \rangle$ and $\langle PE_{H_2O} \rangle$ are the average potential energy of the system (per mole of reverse micelles) and of a single water molecule in the system (per mole of water molecules). ó errors in the last decimal place are shown in parentheses.

and 2 ps during the production runs. This fixed the average temperature at 300.0 K in all of the simulations. Properties were computed from configurations saved at 100 fs intervals.

For comparison with the micelle results, we have also performed simulations of SPC/E water alone inside spherical hydrophobic cavities of different sizes and bulk SPC/E water with periodic boundary conditions. The bulk simulation employed the Ewald summation to evaluate the long-range interactions. In both cases the step size was 2 fs, and the temperature was controlled using the Berendsen thermostat with a time constant of 2 ps.

Table 2 presents parameters and properties for all of the simulations discussed in this paper. Errors were estimated through the usual procedure of performing averages over subblocks of configurations.[84] The results of repeating the entire construction and simulation procedure are shown for $w_0 = 1$, 2, and 4. Results are discussed in the following section.

4. Results

Before embarking on a comprehensive analysis of the simulation results, it is useful to describe the overall picture of the reverse micellar interior that emerges.

Figure 3 presents snapshots of several micelles of different size along with cuts that reveal the structure of the interior. In the smallest micelles, illustrated by the $w_0 = 1$ snapshot, nearly all of the counterions reside on the surface and are triply coordinated by headgroup anions, forming a tightly packed, rigid lattice. This lattice also incorporates a small number of water molecules that modify the triple coordination structure. At $w_0 = 4$ the higher surface density of water interrupts the lattice, leaving a significant number of counterions singly or doubly coordinated. A small fraction of counterions (~10%) form solvent-separated ion pairs or dissociate from the surface altogether. It can also be seen that the spacing between the headgroup anions is not uniform, and thus an important feature of the model is that these ions are allowed to move on the surface of the interface. By $w_0 = 10$ the surface lattice structure has almost completely dissolved, the density of water at the interface exceeds that of the bulk, and about 30% of the counterions are solvent-separated or dissociated. Triply coordinated ions do occur but rarely.

The cuts reveal the structure of the interior, which is composed primarily of water. Three distinct regions of water can be identified based on structural and dynamical properties. While the properties of each region vary substantially with micelle size, a sharp contrast between regions at a given w_0 is maintained at all sizes studied. Following previous nomencla-
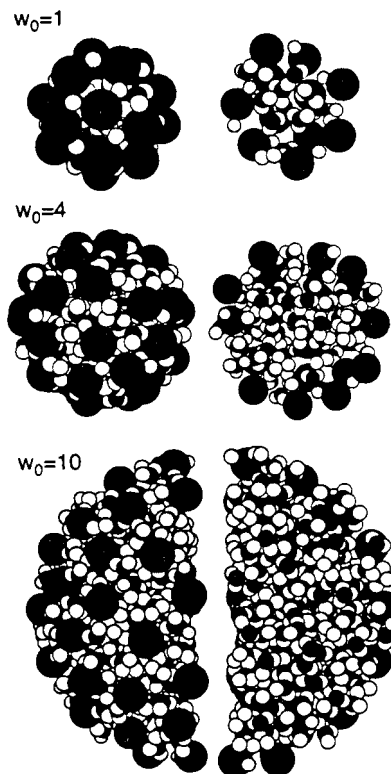

Figure 3. Snapshots of the reverse micelle interior. The headgroup anions are the large, black circles, the Na$^+$ counterions are the small, light gray circles, the water hydrogens are white, and the water oxygens are dark gray. The left-hand side shows the interior surface, which displays the structure of the ionic layer, while the cuts on the right-hand side reveal the interfacial layer and the aqueous core.

ture,[86] we identify a layer of *trapped* water at the interface, a layer of *bound* water attached to the interface, and label the remaining water in the core region as *free* to indicate that water more than a few molecular layers from the interface quickly regains its bulk characteristics.

The strong interaction between water and the surface ions, which disrupts the water hydrogen-bonding network, is the primary force that determines the properties of water at the interface. The layer of ions and water trapped in the interface is rigid because of the high charge density. Each water molecule is multiply coordinated by ions, resulting in low mobility and little hydrogen bonding with other water molecules. Because the headgroup anions are constrained to lie on the surface of a sphere, the interface is sharp and the trapped layer is only one molecular diameter (~3 Å) thick. Most of the water molecules
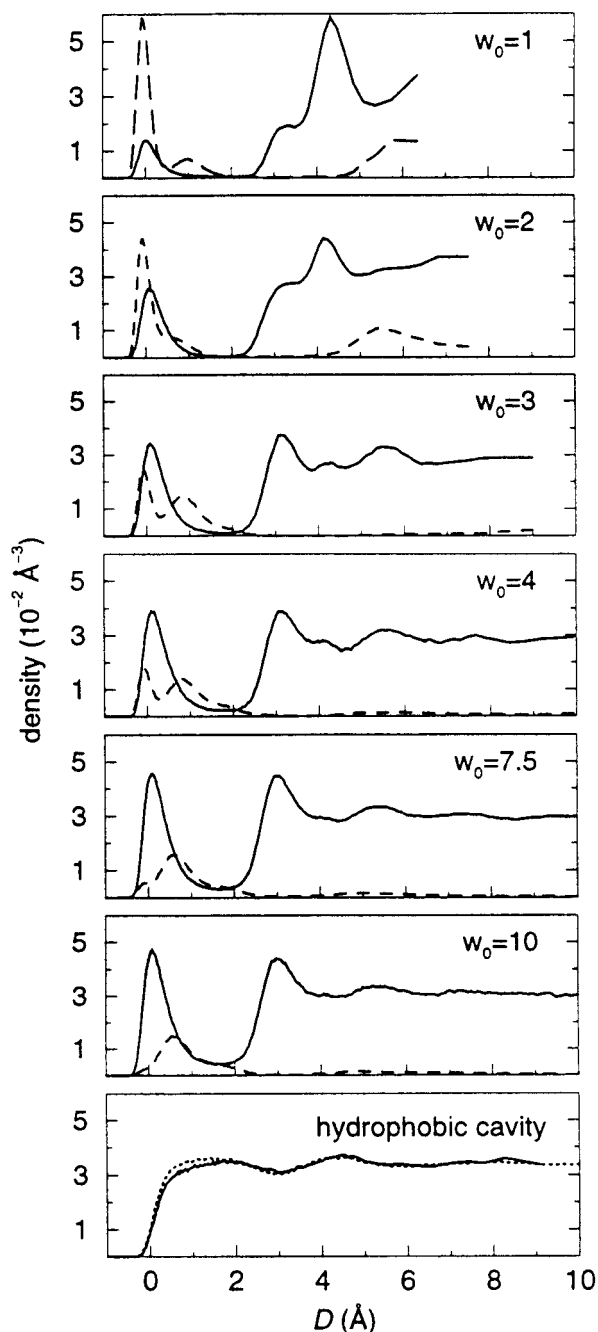
Figure 4. Density of water oxygen atoms (solid lines) and Na^+ ions (dashed lines) as a function of the distance from the interface. Solid and dotted lines in the bottom panel are oxygen densities for HC174 and HC674, respectively. D is measured from the surface 2.5 Å inside the cavity boundary where the hydrophobic potential becomes repulsive.

TABLE 3: Fraction of Counterions and Water in Each Region Based on Radial Density Profiles

| species | w_0 | | | | | |
region	1	2	3	4	7.5	10
Na^+						
lattice[a]	0.80	0.74	0.49	0.41	0.31	0.25
diffuse[b]	0.16	0.15	0.49	0.53	0.58	0.59
free[c]	0.05	0.11	0.02	0.05	0.11	0.16
H_2O[d]						
trapped[e]	0.28	0.32	0.33	0.33	0.22	0.19
bound[f]	0.62	0.49	0.39	0.37	0.31	0.26
free[f]	0.10	0.19	0.28	0.30	0.47	0.55
w_{pert}[g]	0.90	1.62	2.16	2.78	3.98	4.51

[a] $D < 0.5$ Å. [b] $0.5 < D < 3$ Å. [c] $D > 3$ Å. [d] Based on O atom position. [e] $D < 1.5$ Å. [f] The bound and free water regions are separated at the third minimum in the density ($D \sim 4-5$ Å). [g] See eq 8.

positions of the headgroup anions (see Figure 2). The density profile of the anions, not shown, is about 0.1 Å wide and centered at $D = 0$. Fractional populations of counterions and water in various regions of the micelle, obtained by integrating the density profiles, are shown in Table 3.

The radial density profiles for water demonstrate the layering of water near the interface. For all of the micelles there is a well-separated peak in the water oxygen density centered near $D = 0$ that corresponds to water trapped at the interface. The density of the trapped water increases greatly with micelle size, undergoing a nearly 4-fold increase over the range studied. The narrow, approximately 1 Å width of the peak, and the nearly total exclusion of water between the first two layers suggest that water at the interface is tightly bound and highly ordered.

The layer of bound water is reflected by peaks at 3 and 4 Å in the density profiles. For $w_0 = 1$ and 2 the peak at 4 Å corresponds to the region of highest water density within the micelles. These peaks are closely correlated with the distribution of counterions at the interface. The relative intensities of both water and counterion peaks in these small micelles vary substantially between runs. As mentioned earlier, there are different structural isomers for the ionic layer that do not interconvert on several hundred picosecond time scales at 300 K. The water peak at $D = 3$ Å strongly correlates with the size of the counterion peak at $D = 1$ Å, while the water peak at $D = 4$ Å correlates with the counterion peak at $D = 0$. In the large micelles, the $D = 4$ Å peak becomes less pronounced, reflecting the broader counterion distribution and the overall decrease in counterion density. The peak at $D = 3$ Å, nevertheless, remains distinct and appears to increase and shift slightly toward the interface with increasing micelle size.

The exact cutoff of the bound water region is somewhat arbitrary, but it is reasonable to use the position of the minimum after the $D = 4$ Å peak, which ranges from about 5.5 Å for $w_0 = 1$ to just over 4 Å for $w_0 = 10$. There is additional structure in the density profiles beyond this point, most notably a peak at about 5−6 Å, but as we will see below, the effect of the interface on water properties decays rapidly beyond the second molecular layer.

The fraction of water in the free region increases greatly with micelle size, starting from about 10% at $w_0 = 1$ (only a few water molecules) and hitting 55% at $w_0 = 10$. Many experimental studies provide a quantity related to the fraction of free water, which is the number of water molecules per headgroup that are strongly perturbed by the interface. We approximate this number, w_{pert}, based on the total fraction of water in the

in the adjacent molecular layer are bound to at least one surface ion, resulting in reduced mobility and a hydrogen-bonding structure that is intermediate between trapped and free water. The mobility and hydrogen-bond network characteristic of bulk water reemerge within a few molecular diameters from the interface. In the larger micelles, $w_0 = 7.5$ and 10, there are large pools of bulklike free water on the interior despite the high ionic conentrations only a few molecular layers away.

In the following sections we present a detailed analysis of the simulations to expand on this basic picture and make comparisons with experiments and other interfacial systems.

4.1. Radial Density Profiles. Figure 4 shows the number density of water oxygen atoms and Na^+ ions as a function of D, the distance from the interface as defined by the equilibrium

trapped and bound regions:

$$w_{\text{pert}} = w_0(f_{\text{trapped}} + f_{\text{bound}}) \tag{8}$$

The values of w_{pert} obtained by the simulations are shown in the last row of Table 3. Experimental studies report a limiting value of about 6 for large reverse micelles, although values in the range 3−12 have been reported.[5,48] $w_0 = 10$ is not large enough to estimate the limiting value from the simulations.

The density profiles of water in hydrophobic cavities of different size are shown in the bottom panel of Figure 4. To facilitate comparison with the reverse micelle density profiles, D is measured from the surface 2.5 Å inside the cavity boundary where the hydrophobic potential becomes repulsive. These profiles demonstrate that the highly perturbed water structure in the reverse micelles is due almost entirely to presence of ions at the interface. Very little water penetrates the repulsive region of the hydrophobic potential in contrast to the reverse micelles, where the trapped water peak is centered at $D = 0$. Our results for water in spherical hydrophobic cavities are very similar to those of Zhang et al.,[87] who used a flexible SPC model. The weak oscillations in the density profile beyond 4 Å in the reverse micelles are similar in magnitude to those seen in the hydrophobic cavities.

The surface lattice structure is reflected by the sharp counterion peaks at $D = 0$ in the $w_0 = 1$ and 2 micelles. As we discuss in more detail below, the ions in this layer are highly coordinated and tightly bound to the interface. The intensity of this "lattice" peak decays monotonically with increasing micelle size, essentially disappearing by $w_0 = 10$. Even at $w_0 = 1$ the counterion distribution near the surface is bimodal, with a secondary "diffuse" surface state centered at about $D = 1$ Å. The ions in this region are on average bound to fewer anions and have more interactions with water. Table 3 shows that the fraction of counterions in the highly coordinated lattice state declines sharply in favor of the diffuse state after $w_0 = 3$. The width of the diffuse counterion distribution increases up to about $w_0 = 4$, but the distribution appears to hit a cutoff at $D \sim 2$ Å. For all micelle sizes there is a 1−2 Å range beyond $D = 2$ Å of very low counterion concentration that coincides with the region of bound water.

The concentration of counterions in the core decreases with increasing micelle size, but the total fraction of dissociated counterions is actually largest at $w_0 = 10$. For $w_0 = 1$ only a single counterion (~5%) dissolves in the core, while about 16% of counterions dissociate at $w_0 = 10$, corresponding to a core ion density of 1 mol/L.

4.2. Pair Distributions. The various pair radial distribution functions and associated coordination numbers provide a more detailed view of the ion and water structure. For simplicity and to facilitate the comparison between different micelle sizes, we have plotted the unnormalized pair density instead of the usual pair distribution function.[84] For a given pair of species A and B, the pair density $\rho_{AB}(r)$ is defined such that $4\pi\rho_{AB}(r) r^2 \, dr$ is the average number of species B that are between r and $r + dr$ away from species A. Thus, if ρ_B is the average number density of B in the system, $\rho_{AB}(r) = \rho_B g_{AB}(r)$, where $g_{AB}(r) = g_{BA}(r)$ is the usual pair distribution function between A and B. The problem with using $g_{AB}(r)$ for the ion pair distributions is that the total ion density varies with w_0, making it difficult to compare distributions for different micelle sizes.

Figure 5 shows the Z^-−Na$^+$ radial pair density functions (pdf's) and running coordination numbers for $w_0 = 1$, 4, and 10. Table 4 shows the coordination numbers of the headgroup anions with both Na$^+$ and H$_2$O. These data quantify the picture
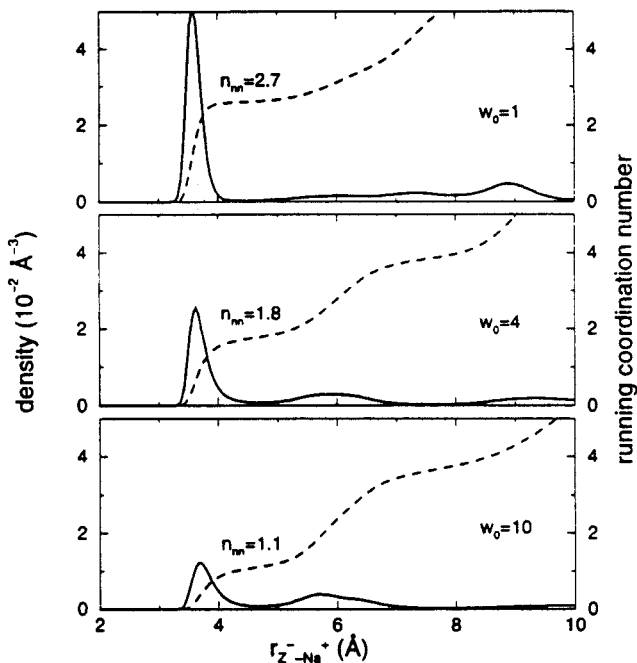

Figure 5. Z^-−Na$^+$ pair densities (solid lines) and running coordination numbers (dashed lines). n_{nn} is the number of ions in the first coordination shell.
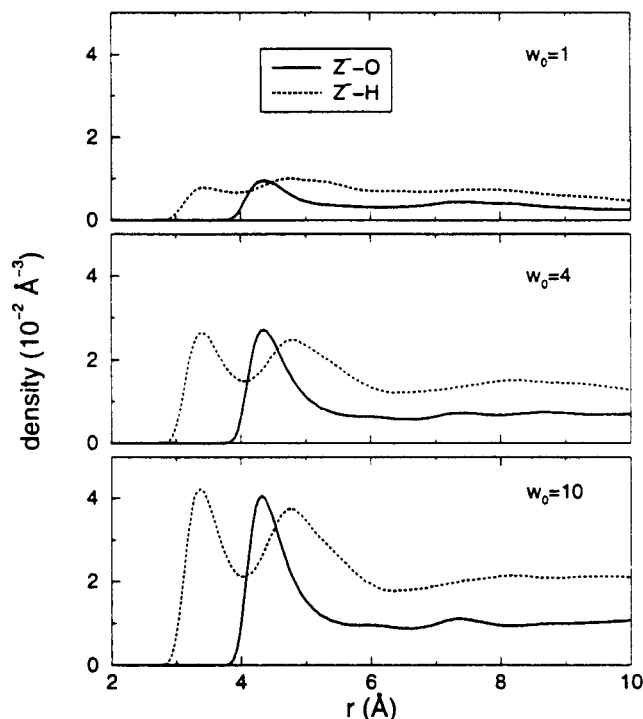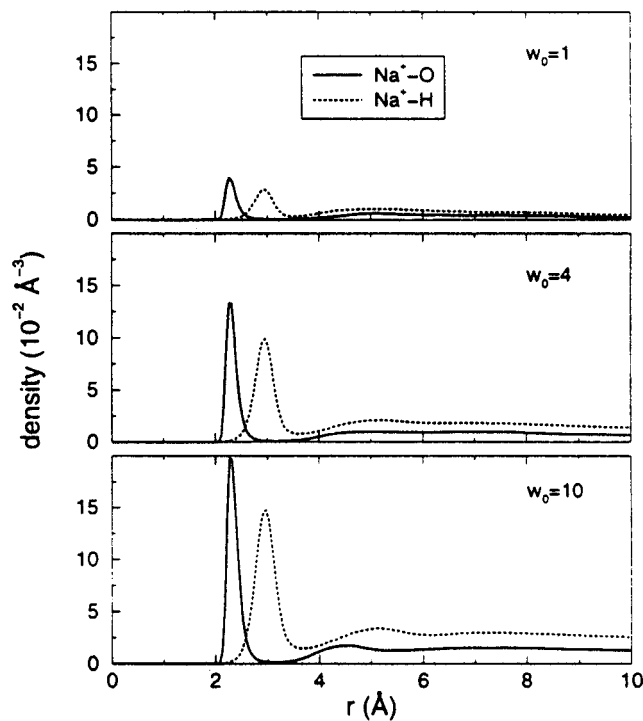
TABLE 4: Head Group Anion Coordination Numbers

	w_0					
interaction	1	2	3	4	7.5	10
Z^-−Na$^{+\ a}$	2.7	2.2	2.2	1.8	1.4	1.1
Z^-−O^b	1.9	3.4	4.3	4.9	6.7	7.2
Z^- H-bond^c	1.1	2.1	2.4	3.1	4.3	4.9

^{a} $r_{Z^-\text{Na}^+} < 4.8$ Å. ^{b} $r_{Z^-\text{O}} < 5.0$ Å. ^{c} $r_{Z^-\text{H}} < 4.0$ Å.

of ion structure and water penetration presented above. The sharp peak in the $w_0 = 1$ pdf and the Z^-−Na$^+$ coordination number of nearly 3 indicate that a rigid, triply coordinated lattice forms at the reverse micellar interface. This peak becomes broader and the Z^-−Na$^+$ coordination number falls as the micelle size increases, reaching a value of about 1 at $w_0 = 10$. These trends reflect the decrease in ion density at the interface that breaks up the lattice and allows water molecules to penetrate the surface layer. The development of a distinct secondary peak in the ion−ion pdf near 6 Å and the increased counterion mobilities, described below, also demonstrate the much more fluid nature of the ionic layer in the larger micelles.

Figure 6 shows the Z^-−O and Z^-−H pdf's, revealing a strong water orientation indicative of hydrogen bonding. The hydrogen bonding to water protons is evident in the Z^-−H pdf's at all sizes, but the total density in the first solvation shell increases greatly with w_0. At $w_0 = 1$ each Z^- has only about 2 water molecules near neighbors, while this number increases to over 7 at $w_0 = 10$. The average number of Z^-−water hydrogen bonds closely tracks the values of w_{pert}, suggesting that our definition of perturbed water, which was based solely on the density profiles, is a reasonable one. The number of hydrogen bonds is always greater than w_{pert} because some trapped water molecules hydrogen bond to more than one anion. The fact that the Z^-−O coordination numbers are much larger than the hydrogen-bonding numbers indicates that there is substantial overlap of the Z^- hydration shells.

The Na$^+$−water pdf's plotted in Figure 7 show the expected orientation of the water protons away from the cations. The sharp peak in the Na$^+$−O pdf's and the near zero density in

Figure 6. Z^-—H_2O pair densities.

Figure 7. Na^+—H_2O pair densities.

the region between the first and second solvation shells reflect the much stronger interaction between the water and the relatively small cations. The profiles, particularly at $w_0 = 10$, are quite similar to the Na^+—water pdf's at infinite dilution,[80] which shows that the presence of other nearby ions does not disrupt the pair coordination structure. The density of counterion—water pair interactions also undergoes a dramatic increase with micelle size, reflecting the breakup of the ionic lattice and the increasing penetration of water.

The counterion coordination numbers for counterions in the three different states— lattice, diffuse, and free— are listed in Table 5. Counterions in the lattice state coordinate on average

TABLE 5: Counterion Coordination Numbers by Counterion Region (Based on Classification in Table 3)

species	w_0					
region	1	2	3	4	7.5	10
Z^- [a]						
lattice	2.9	2.6	2.7	2.5	2.1	1.8
diffuse	2.3	1.9	1.8	1.4	1.3	1.1
free	0.0	0.1	0.1	0.1	0.1	0.1
H_2O [b]						
lattice	0.1	0.6	0.7	0.9	2.0	2.5
diffuse	2.2	2.5	2.8	3.4	3.6	3.9
free	5.7	5.7	5.5	5.6	5.7	5.7

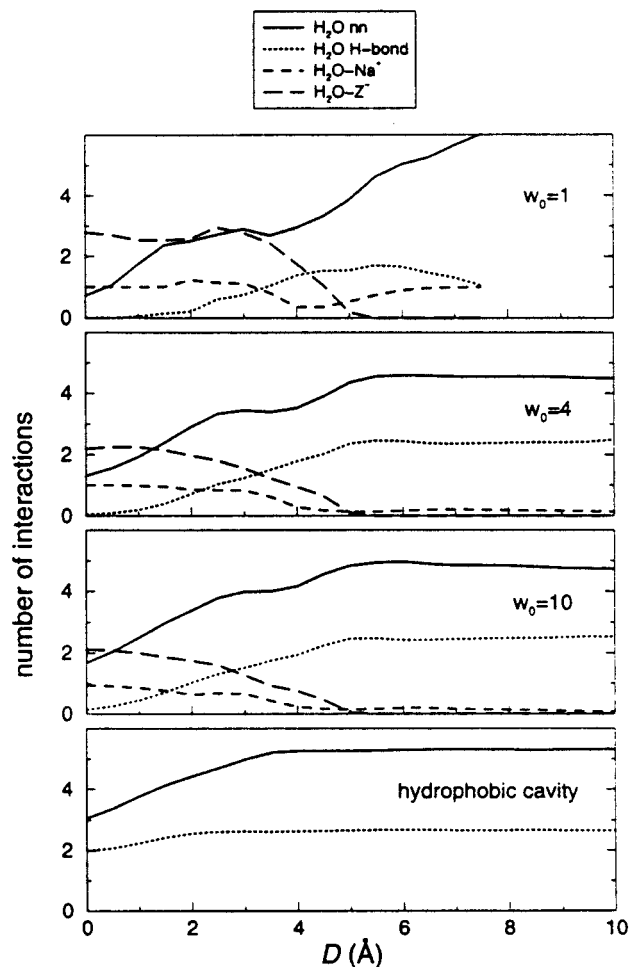[a] $r_{Na^+-Z^-} < 4.8$ Å. [b] $r_{Na^+-O} < 3.5$ Å.

Figure 8. Water—ion and water—water interactions as a function of distance from the interface. The cutoffs for the water—water nearest neighbor, Na^+ coordination, and Z^- coordination are $r_{Q-Q} < 3.5$ Å, $r_{Q-Na^+} < 3.5$ Å, and $r_{Q-Z^-} < 5.0$ Å, respectively. The water—water hydrogen bond energy threshold is -16 kJ/mol. The hydrophobic cavity results are from HC674. The properties are computed in 0.5 Å wide bins.

more anions and fewer water molecules than those in the diffuse state, supporting the distinction suggested by the radial density profiles. For counterions in both of these states, the drop in anion coordination and the rise in water coordination are monotonic with micelle size. Counterions in the free region have nearly identical coordination numbers as ions at infinite dilution.[80]

Figure 8 shows the water—ion and water—water coordination numbers as a function of D. Near the interface water interactions are dominated by the ions. Water molecules in the trapped region essentially do not hydrogen bond to other water molecules, while

hydrogen bonding in the bound region is reduced by a factor of 2. The amount of water−water hydrogen bonding near the interface goes up only slightly with micelle size despite the substantial increase in the water concentration. This disruption of the water−hydrogen bond network near the interfaces contrasts with the relative increase in hydrogen bonding near the interface of the hydrophobic cavity. While the number of nearest-neighbor interactions at the hydrophobic interface drops by a factor of 2, the average number of hydrogen bonds falls by only about 20%. This relative enhancement of hydrogen bonding near the interface is a well-known feature of hydrophobic surfaces.[26]

Near the interface, the water−water interactions are replaced by ion−water interactions. Figure 8 shows that trapped water is surrounded by a highly ionic environment including several anions and a cation. The water molecules must adopt specific orientations in order to have simultaneously favorable interactions with its ionic neighbors. Water in the bound region still tends to have multiple ionic interactions, but the coordination numbers drop sharply in this region. This drop is particularly large for the Na^+ coordination between 3 and 4 Å and has a substantial effect on the average water orientation discussed below.

Except for the $w_0 = 1$ micelle, the water−ion coordination falls to nearly zero and the water−water coordination reaches a plateau at a point that coincides with the definition of the water core based on the radial density profiles. The water density in the core is about 10% lower than that in the bulk, which accounts for the slightly lower amount of water−water coordination and hydrogen bonding compared to the interior of the hydrophobic cavity. The significant counterion concentration in the core probably accounts for these differences, which are quite small compared to the structural changes at the interface.

4.3. Water Orientation. In this section we present several measures of the water orientation near the ions and the interface. Figure 9 shows the angular distribution of the water OH bond and the dipole moment relative to the intermolecular separation vector for water in the first hydration shells of Na^+ and Z^-. In all cases, the electrostatic interactions determine the most likely orientations: the dipole moment and the protons point away from the cation and toward the anion. The angular distributions do not vary greatly with micelle size. The angular distributions with Na^+ are sharper because the cations are so much smaller than the anions and also because of the overlap between the anion hydration shells. While each water molecule is on average coordinated by several anions, it appears to hydrogen bond with only one. This overlap does not, however, cause water to adopt less favorable conformations with respect to Na^+.

Figure 10 shows the angular distribution of the water dipole with respect to the cavity interface as defined by the outward pointing surface normal. The $D = 0$ profile shows that the dipole of trapped water orients toward the surface, an effect that increases with w_0. The electrostatic field created by the ions favors this alignment because the cation density is centered at $D > 0$, moving inward as w_0 increases. In the hydrophobic cavities, the water dipole also exhibits some preferential outward orientation, but the origin of this effect is not clear. Significant orientation is also observed in the $D = 3$ and 4 Å micelle distributions, while there is little orientation at these distances from the hydrophobic interface. The angular distribution at $D = 3$ Å is bimodal for $w_0 = 4$ and 10, with a peak at $\cos \theta_{dip} = -1$. This peak arises from water molecules that are coordinated with counterions in the diffuse state, which is a small fraction of counterions at $w_0 = 1$. At $D = 4$ Å the distribution strongly
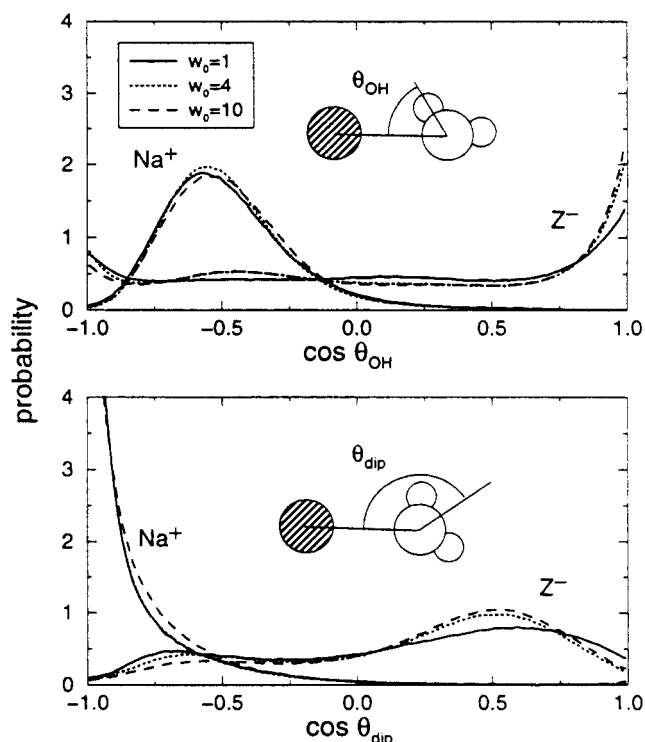

Figure 9. Angular distribution functions of water in the first hydration shell of Na^+ (solid lines) and Z^- (dotted lines) for $w_0 = 1$, 4, and 10. A uniform distribution would have a y value of 0.5.

favors dipole orientation toward the interface because far few water molecules in this region are coordinated by counterions.

The water polarization density is another, perhaps more physically meaningful, way to characterize the water response to the surface charge distribution. The polarization density is given by[88]

$$\vec{\mathcal{P}}(\vec{R}) = \vec{m}(\vec{R}) - \vec{\nabla} \cdot \mathbf{P}(\vec{R}) \qquad (9)$$

where $\vec{m}$ is the dipole moment density and $\mathbf{P}$ is the quadrupole density tensor, the radial projections of which are both easily calculated from the simulations. Figure 11 plots both the polarization and dipole moment densities projected along the outward radial direction as a function of distance from the interface. In the trapped water region, both the total polarization and the dipole densities increase substantially as a function of micelle size. The polarization drops to nearly zero between the trapped and bound layers and rises again in the bound region, undergoing several oscillations where the water coordination structure changes most substantially. The bound layer shifts toward the interface as w_0 increases. The dipole density shows a small bump in the core region at around 6 Å before decaying completely to zero at about 10 Å. There is less structure in the core polarization density, and it drops below zero near 10 Å, appearing to diverge near the micelle center. The polarization of water in the core, however, is zero beyond 10 Å because of the R^2 dependence of the volume element. It interesting that the hydrophobic cavity also displays significant polarization at the interface, apparently as a byproduct of the enhanced hydrogen-bonding structure. For all of the systems studied the quadrupole moment density makes a substantial contribution to the total polarization density.

The polarization density profile of the reverse micelles shows the distinct separation between the two primary water layers and differs quite markedly from the distribution shown in Figure 8 of ref 32, which, though bimodal, does not display a region
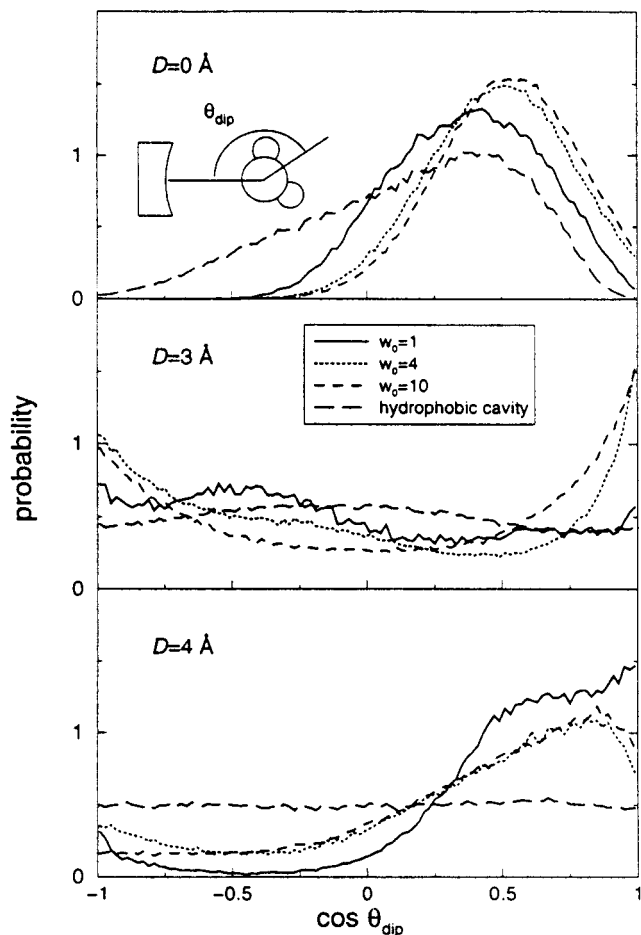
Figure 10. Angular distribution functions of the water dipole with respect to the outward pointing surface normal at several distances from the interface. Bins of 0.5 Å thickness were used for each *D* value.

Figure 11. Water radial polarization densities (solid lines) and dipole moment densities (dotted lines) in reduced units μv_0 as a function of the distance from the interface. μ is the molecular dipole moment of water in the SPC/E model, 2.35 D, and v_0 is the molecular volume of water, 30 Å³.

of very low polarization between the layers. The differences in the polarization density profiles mirror those in the radial density profiles and arise from differences in the models of the interface, which are described in section 3. The two water layers are more distinct in the current model. As mentioned earlier, we expect the current model to provide a more accurate description of the interface in an AOT reverse micelle because the ion density is closer to that observed in the experiments and because surface charges are not scaled.

4.4. Translational Mobilities. We now turn from a static description of the reverse micelles to examine several basic dynamical properties. A simple measure of the translational mobility within the cavity is given by the mean-squared center-of-mass displacements (msd's). At long times these displacements can be related to the diffusion coefficient by the Einstein relation

$$D = \lim_{t \to \infty} \frac{\langle |\mathbf{R}(t) - \mathbf{R}(0)|^2 \rangle}{6t} \tag{10}$$

where $\mathbf{R}$ is a vector containing the center-of-mass coordinates of the species being examined. For a confined system, the diffusion coefficient is zero, but it is possible to define an effective diffusion coefficient over the time scales on which the msd's are linear. Figure 12 shows msd's for water in different regions of the $w_0 = 10$ reverse micelle and the larger hydrophobic cavity. The most striking difference between the two is that mobility decreases sharply near the reverse micellar interface, while mobility actually increases near the hydrophobic
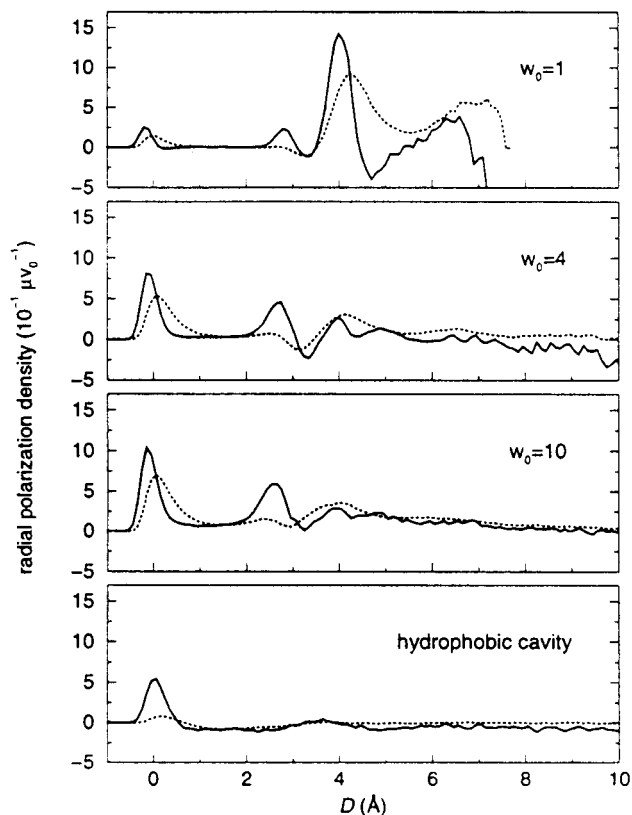
surface. The latter effect has been observed in other simulations of hydrophobic interfaces with both flat[27] and cylindrical[89] geometries. The water mobility in the core nears the bulk value in both systems, although in both cases the core mobility is higher than the mobility in the bulk. In the hydrophobic cavity the enhancement may be due to molecules that diffuse into the interfacial regions being included in the average. The enhancement is quite small in the reverse micelle and may result from a water density that is about 10% lower in core than in bulk water.

The water mobilities are quantified by the effective diffusion coefficients reported in Table 6. These are determined from the slope of a linear fit to the msd's between 2 and 10 ps. While the enhancement of the water mobility at the hydrophobic surface is roughly 25%, much larger differences are observed among the trapped, bound, and free water regions of the reverse micelles. Water in the bound region is much more mobile than trapped water and has a mobility closer to that of the free water, although the difference in mobility between the bound and free water increases with w_0. The water mobility within each region increases with micelle size. The mobility change is largest for trapped water, which is about an order of magnitude less mobile in the $w_0 = 1$ micelle than in the $w_0 = 10$ micelle.

Effective counterion diffusion constants have also been determined in the same way and are listed in Table 7. As expected, ions at the surface are much less mobile than the free ions in the core. In the smallest micelles, the mobilities of the lattice counterions are 50−100 times smaller than those in the bulk, and 20−30 times smaller than the free ion mobilities. There is also a significant difference between ions in the lattice and diffuse states. These differences disappear in the larger
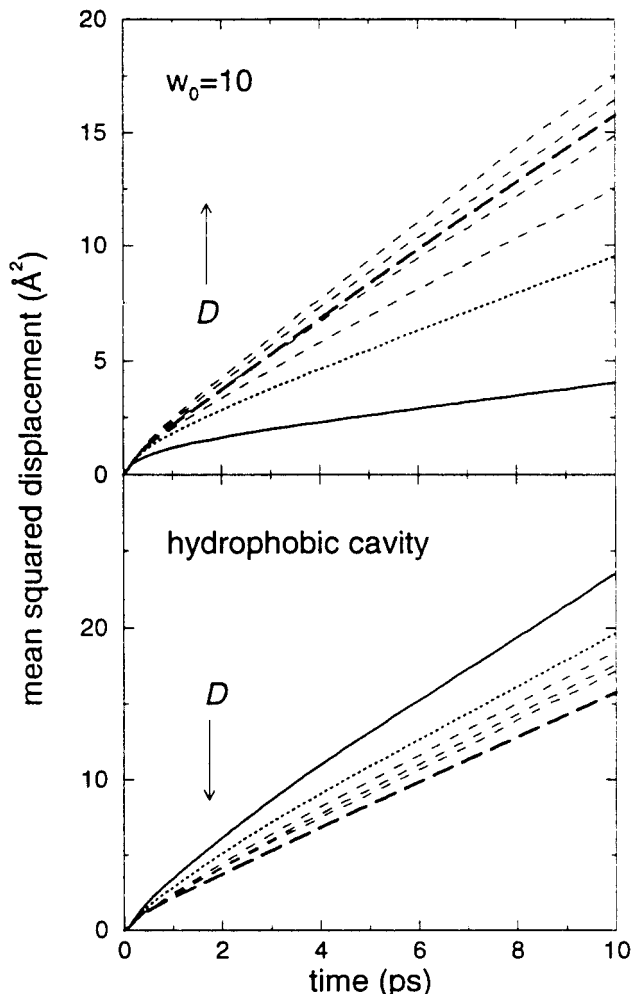
Figure 12. Mean-squared displacement of water by region within the $w_0 = 10$ micelle and HC674. The displacements of water in the trapped, bound, and free regions are shown by solid, dotted, and thin dashed lines, respectively. The position of each molecule at the time origin determines the average to which it contributes. The same D values are used to define the regions in both cavities. The free water region is divided into 3 Å wide bins out to 13.5 Å. The water region furthest from the interface in the reverse micelle contains all water molecules with $D > 13.5$ Å. The displacements increase monotonically with the distance from the interface in the reverse micelle but decrease with D in the hydrophobic cavity. The thick dashed lines show the displacement of bulk water in the B216 simulation.

TABLE 6: Effective Water Diffusion Coefficients[a] by Region[b] from Mean-Squared Displacements[c] (10^{-9} m² s⁻¹)

region	w_0						HC[d]	
	1	2	3	4	7.5	10	174	674
trapped	0.05	0.04	0.18	0.28	0.36	0.50	3.5	3.6
bound	1.05	1.01	1.03	1.16	1.25	1.38	2.8	3.0
free I[e]	0.84	0.96	1.61	1.76	1.86	1.90	2.7	2.9
free II[f]			1.83	2.23	2.23	2.30	2.8	2.8
free III[g]					2.51	2.57		2.7
free IV[h]						2.75		

[a] Based on linear fits for $t = 2-10$ ps. [b] Molecules tagged according to the $t = 0$ position. [c] D_{bulk} from B216 is 2.50×10^{-9} m² s⁻¹. [d] HC regions are based on a reverse micelle of similar radius. [e] $4.5 < D < 7.5$ Å. [f] $7.5 < D < 10.5$ Å. [g] $10.5 < D < 13.5$ Å. [h] $D > 13.5$ Å.

micelles, but the surface ions overall remain far less mobile than the free ions. The free ions in the largest micelles are about 50% less mobile than those in the bulk at infinite dilution, probably because of the relatively high ion concentration in the core.

TABLE 7: Effective Counterion Diffusion Coefficients[a] by Region[b] from Mean-Squared Displacements[c] (10^{-9} m² s⁻¹)

region	w_0					
	1	2	3	4	7.5	10
lattice	0.01	0.02	0.05	0.08	0.16	0.21
diffuse	0.06	0.07	0.11	0.15	0.22	0.27
free	0.31	0.39	0.59	0.74	0.65	0.76

[a] Based on linear fits for $t = 2-10$ ps. [b] Counterions tagged according to the $t = 0$ position. [c] Bulk value for SPC/E water at 298 K is 1.28×10^{-9} m² s⁻¹ from ref 80.

TABLE 8: Water Residence Times at the Interface in picoseconds

region	w_0						HC 674
	1	2	3	4	7.5	10	674
trapped	236	77	56	34	45	34	1.7
bound	41	36	26	20	19	18	1.7

Mobility can also be characterized by lifetimes of molecules in the various regions. One way to define the survival probability of a molecule is the probability that a molecule in a given region of the cavity at time zero occupies that region continuously until time t. The survival probabilities are easily computed from the simulations, and residence times are then determined by integrating these from $t = 0$ to ∞. Ion residence times in even the largest micelle are too long to be determined in our simulations, but the water residence times are shown in Table 8. As with the diffusive mobilities, the residence times decrease within each region as the micelle size increases, and there is a substantial difference between the trapped and bound residence times at all sizes. The residence times for both of these regions in the reverse micelles greatly exceed those of water in the same regions of the hydrophobic cavity. The residence times of bound water in even the largest micelle are an order of magnitude longer than those of the hydrophobic cavity, which suggests that a larger portion of the mobility in the micellar systems occurs within the layers parallel to the interface.

4.5. Rotational Mobilities. The rotational mobility of water can be measured by computing the dipole−dipole autocorrelation function,

$$C(t) = \frac{\langle \vec{\mu}(0) \cdot \vec{\mu}(t) \rangle}{\vec{\mu}^2} \qquad (11)$$

which is plotted in Figure 13 for water in the three main regions of the reverse micelles and the smaller hydrophobic cavity (the results for HC674 are nearly identical). The rotational mobility trends are essentially the same as those observed for the translational diffusion. The dipole reorientation is very slow at the interface but increases sharply in the bound layer and grows still further in the core, while there is almost no difference in rotational mobility among the regions of the hydrophobic cavity. The mobility within each layer also increases with micelle size. The reorientation of water in the reverse micelles is highly nonexponential, involving a long-lived tail that is pronounced in all regions but becomes very large near the interface. The reorientation is complicated by the movement of molecules among the different regions of the micelle, which occurs on a similar time scale. The reorientation at the interface is enhanced by molecules moving out of the interfacial region, while the mobility on the interior appears slower because some molecules migrate to the interface, where they are essentially frozen. Because of the coupling between translation and rotation, we do not attempt to compute reorientation times, but we note that
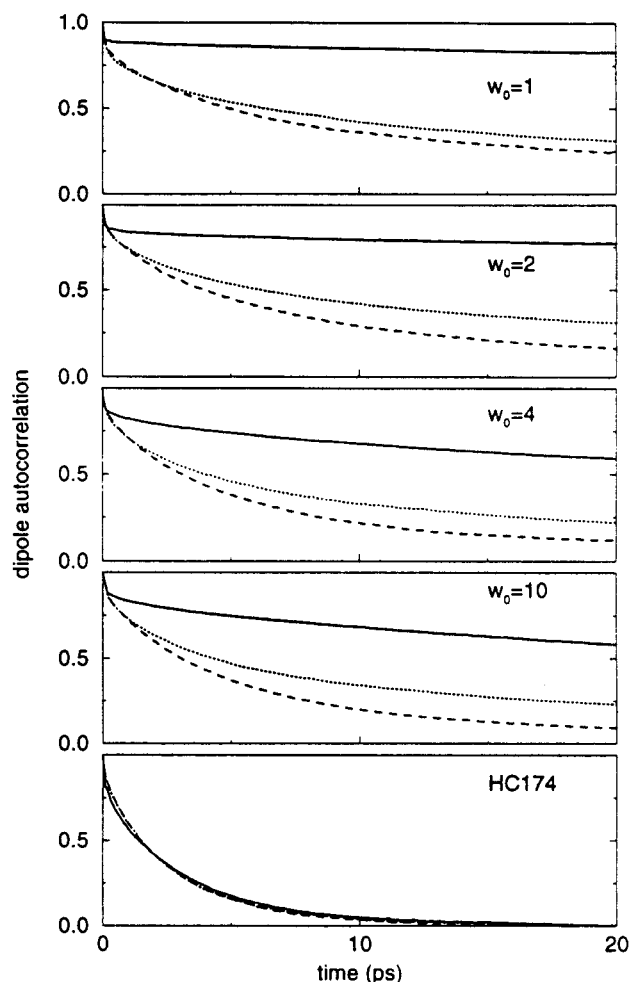
Figure 13. Dipole−dipole autocorrelation functions of water by region within the micelle. The solid, dotted, and dashed lines correspond to trapped, bound, and free water, respectively. The classification of each molecule at the time origin determines the average to which it contributes.

the time scale for reorientation near the interface is tens to hundreds of picoseconds. The differences between reorientation at the interface and in the core are much larger than those observed by Linse[32] because of the much higher ion densities and ionic charges in our model.

On a cautionary note, it is tempting to conclude from these results that a process, such as the solvation dynamics of a probe molecule, that involves significant motion of water molecules will have substantial long-time components arising from the restriction of translational and rotational motion described here. Preliminary simulations by us[90] of the collective dipole response and solvation dynamics of a diatomic probe ion indicate that, in fact, the collective response is much faster than expected. Unlike the single molecule motions described above, the collective response appears to be quite similar to that of bulk water because the collective motions are highly cooperative and involve both ions and water. One does expect to see some effects from the restriction on molecular motion, but these seem to show up as a relatively small fraction of the collective response (∼10−20%), which is relatively difficult to detect in these molecular simulations.

5. Discussion

5.1. Comparisons with Other Simulations. Our results are consistent with other simulations of water at a broad range of interfaces. As we saw in the results for the hydrophobic cavity, the water density profiles near weakly interacting interfaces show little structure.[26,27,89,91−93] The density profiles for water near many different types of strongly interacting interfaces show pronounced peaks and valleys indicative of ordered layer formation.[27,28,30,35,89,94] The effect of the water−wall interaction strength has been examined by Hartnig et al.,[89] who showed that layering could be induced simply by increasing the interaction strength while holding the form of the potential constant. A similar contrast has also been observed in the relative amounts of hydrogen bonding at hydrophobic and hydrophilic interfaces. Hydrogen bonding is enhanced near weakly interact-ing interfaces[26,27,91] and sharply reduced at hydrophilic[27,95,96] and polar interfaces,[29,32] a trend nicely illustrated by the water−hydrogen bond profiles in Figure 8. Water mobility trends are also opposite for the two different classes of interface. Trans-lational mobility is enhanced near hydrophobic interfaces[27,89,91] and greatly reduced in the first several solvation shells of hydrophilic ones.[27,32,89,96] In our simulations, rotational mobility is not significantly affected by the hydrophobic interface but is sharply reduced in the regions near the surfactant headgroups. Similar reductions in the rotational mobilities of water have been observed in simulations of reverse micelles,[32] surfactant mono-layers,[97] and the protein−water interface.[36]

The present simulations also fit with the nearly universal previous observation that the dynamical and structural changes of water near the interface fall off rapidly over a span of a few molecular layers, regardless of the interaction strength.[27−29,32,89,96] The clearest evidence for the short range of structural changes in the present simulations can be found in the water density and hydrogen bond profiles. Similar trends are observed in the reduction of water mobility near the interface. Typical estimates for the reduction of mobility near strongly hydrophilic interfaces are a factor of 2−10,[27,96,97] although the change may be difficult to quantify because the nature as well as the magnitude of the diffusive motion is affected.[36] For example, we do not attempt to estimate rotational relaxation times because of the very long time scale for trapped water relaxation and the highly nonex-ponential nature of the decay. We do, however, see a reduction in the mobility of trapped water in the smaller micelles substantially greater than 1 order of magnitude, which can be attributed to the very high ion densities. Trapped water, though, accounts for at most just a few water molecules per headgroup, and the reduction in the translational mobility of the bound layer is only by a factor of 2−5. The mobility of free water in the micelles large enough to have a core is only slightly diminished and appears to approach the bulk by about $D = 10$ Å. Finally, the polarization profiles shown in Figure 11 show that even for highly polar interfaces most of the electrostatic effects are confined to the first two molecular layers. These results agree well with those of Linse,[32] who studied a less polar interface, and those of Kjellander and Marcelja,[28] who studied a system with an ion density (about 50 Å²/ion pair) comparable to the large reverse micelles.

5.2. Comparisons with Experiment. Comparison with experimental results is complicated by the fact that we have not computed any directly measurable experimental quantities from the simulations. We therefore limit our comparisons to the various qualitative features that been extracted from the experiments. The present simulations support the basic notion that water forms layers on the reverse micellar interior but also cast doubt on whether experiments can accurately quantify the water populations. The basic problem is that in addition to the change in populations the properties of the interfacial water vary

with micelle size because of the constant change in the surface ion density. The broad range of reported headgroup coordination numbers, $2-15$,[5] illustrates the difficulty of using the experiments alone to obtain details at the molecular level. A more intimate connection between molecular modeling and experiments may ultimately provide greater insights into the molecular structure of the interface. Nevertheless, there is a basic agreement between the pictures of water and interfacial structure that emerge from both experiments and the present simulations.

The simulations strongly support the predominant view that interfacial water is characterized by strong interactions with ions, reduced hydrogen bonding, and decreased mobility, while water away from the interface regains bulk characteristics. While we have emphasized the uncertainties surrounding multistate fitting models, the majority of these give results consistent with a perturbed water region extending $1-2$ molecular layers from the interface with populations comparable to those in Table 3.[5,22,23,44,86] Several authors have even found evidence that up to a few water molecules per headgroup are "trapped" at the interface.[23,48] There is a large body of evidence that water mobility, both translational[10,21,65,66] and rotational,[11,49] is greatly reduced inside reverse micelles but increases greatly with micelle size. These trends may be fit by models that assume reduced mobility of interfacial water,[21,48,98] but so far the experiments cannot spatially resolve the mobility. The current simulations support the idea that mobility increases rapidly with distance from the interface. One area of current controversy is the interpretation of IR spectra of the water OH/OD stretching bands. A number of workers have used multi-Gaussian fits of the OH stretch in H_2O or the OD stretch in D_2O along with multistate models to quantify the changes in hydrogen bonding that occur with micelle size.[23,44,45,47,99] Others have argued that the changes in band shape cannot be directly attributed to hydrogen bonding because of intramolecular vibrational coupling and have found that the decoupled OD stretching band of HOD does not exhibit multiple components,[43,67] leading to the conclusion that there is not a substantial spatial variation of water hydrogen bonding within reverse micelles.[52,67] The band shifts they do observe are, however, consistent with reduced hydrogen bonding in reverse micelles and an increase with increasing w_0.[43,67] The current simulations, and many others, suggest that hydrogen bonding is reduced at the reverse micellar interface, and a direct calculation of the IR spectrum from the molecular simulations in the future might help to clear up the current discrepancies. Finally, we note that the range of water perturbation, about 10 Å, is in good agreement with the observations from a wide range of other interfacial systems.[20]

The simulations also support the picture of ion structure that has emerged from IR spectroscopy of sulfonate,[23,46] counterion NMR,[11,50,51] and calorimetry.[62,63] In this picture, at small micelle sizes, the ion density is very high, and the headgroup ions and counterions form a rigid "quasi-lattice"[63] at the interface. As the micelle size increases, the ion density decreases, leading to a breakup of the lattice and water penetration of the interfacial layer, which is endothermic, but entropically favored.[62,63] In the larger reverse micelles, even with the breakup of the ionic lattice, the interaction between sulfonate and counterions remains strong and a large fraction ($\sim70\%$) of the ions remain ion-paired.[11,46]

We hope that the current model will aid interpretation of experimental results and the development of theoretical treatments of the reverse micellar interface, but it will probably have to be extended before quantitative comparisons with experiments can be made. It may be possible to make the interface more realistic by improving the description of the sulfonate headgroup,

but it will also be desirable to simulate the entire extended system at a molecular level in order to determine the accuracy of the reduced models. Such simulations are currently feasible but will require more detailed and systematic analysis than have so far been applied if good comparisons are to be made. As mentioned earlier, some steps in this direction have already been taken.[73] It also may be possible to make such simulations more tractable by using simplified models of the surfactant, such as the one developed by Palmer and Liu.[100] Another simplification that might prove useful in both reduced and extended models would be to vary the surface charge density holding the reverse micelle size fixed. As long as the core region is more than a few molecular diameters across, the effects of the overall size and the curvature should be minimal in comparison to the charge density of the interface.

6. Conclusions

We have characterized the structure and dynamics of water in the interior of reverse micelles of varying size. We find that water forms distinct molecular layers at the interface that are bound to the surface ions and characterized by reduced mobility and hydrogen bonding. The characteristic hydrogen-bonding network returns, however, within a few molecular layers along with other properties of bulk water. The main effect of size variation is to change the relative amounts of water in the various regions, although the properties within each region also vary substantially. The decrease in charge density at the interface as the micelle size increases results in greater fluidity of the interfacial region.

These simulations confirm the basic multistate picture of water near strongly attractive interfaces that has been observed in other simulated systems and invoked to explain a broad range of experimental results. The results do suggest, however, that such models should take into account the variation in properties of each region as well as the changes in composition. Caution is required in employing these ideas to rationalize more collective solvent phenomena, which may be more robust than expected, even in these highly confined systems.

References and Notes

(1) De Gennes, P. G.; Taupin, C. *J. Phys. Chem.* **1982**, *86*, 2294.

(2) Luisi, P. L., Straub, B. E., Eds. *Reverse Micelles*; Plenum: New York, 1984.

(3) Langevin, D. *Acc. Chem. Res.* **1988**, *21*, 255.

(4) Chevalier, Y.; Zemb, T. *Rep. Prog. Phys.* **1990**, *53*, 279.

(5) De, T. K.; Maitra, A. *Adv. Colloid Interface Sci.* **1995**, *59*, 95.

(6) Moulik, S. P.; Paul, B. K. *Adv. Colloid Interface Sci.* **1998**, *78*, 99.

(7) Gelbart, W. M., Ben-Shaul, A., Roux, D., Eds. *Micelles, Membranes, Microemulsions, and Monolayers*; Springer: Berlin, 1994.

(8) Gelbart, W. M.; Ben-Shaul, A. *J. Phys. Chem.* **1996**, *100*, 13169.

(9) Schulman, J. H.; Stoeckenius, W.; Prince, L. M. *J. Phys. Chem.* **1959**, *63*, 1677.

(10) Wong, M.; Thomas, J. K.; Grätzel, M. *J. Am. Chem. Soc.* **1976**, *98*, 2391.

(11) Wong, M.; Thomas, J. K.; Nowak, T. *J. Am. Chem. Soc.* **1977**, *99*, 4730.

(12) Zulauf, M.; Eicke, H.-F. *J. Phys. Chem.* **1979**, *83*, 480.

N *J. Phys. Chem. B* PAGE EST: 13.9

Faeder and Ladanyi

(13) Robinson, B. H.; Toprakcioglu, C.; Dore, J. C. *J. Chem. Soc., Faraday Trans. 1* **1984**, *80*, 13.

(14) Kotlarchyk, M.; Huang, J. S.; Chen, S.-H. *J. Phys. Chem.* **1985**, *89*, 4382.

(15) Prince, L. M. *J. Colloid Interface Sci.* **1975**, *52*, 182.

(16) Luisi, P. L.; Giomini, M.; Pileni, M. P.; Robinson, B. H. *Biochim. Biophys. Acta* **1988**, *947*, 209.

(17) Langevin, D. In *Reverse Micelles*; Luisi, P. L., Straub, B. E., Eds.; Plenum: New York, 1984; pp 287−303.

(18) Pileni, M. P. *J. Phys. Chem.* **1993**, *97*, 6961.

(19) Tanford, C. *The Hydrophobic Effect*, 2nd ed.; Wiley: New York, 1980.

(20) Halle, B.; Wennerström, H. *J. Chem. Phys.* **1981**, *75*, 1928.

(21) Zinsli, P. E. *J. Phys. Chem.* **1979**, *83*, 3223.

(22) Maitra, A. *J. Phys. Chem.* **1984**, *88*, 5122.

(23) Jain, T. K.; Varshney, M.; Maitra, A. *J. Phys. Chem.* **1989**, *93*, 7409.

(24) Israelachvili, J. N. *Intermolecular and Surface Forces*, 2nd ed.; Academic Press: New York, 1992.

(25) Geiger, A.; Rahman, A.; Stillinger, F. H. *J. Chem. Phys.* **1979**, *70*, 263.

(26) Lee, C. Y.; McCammon, J. A.; Rossky, P. J. *J. Chem. Phys.* **1984**, *80*, 4448.

(27) Lee, S. H.; Rossky, P. J. *J. Chem. Phys.* **1994**, *100*, 3334.

(28) Kjellander, R.; Marcelja, S. *Chem. Scr.* **1985**, *25*, 73.

(29) Kjellander, R.; Marcelja, S. *Chem. Phys. Lett.* **1985**, *120*, 393.

(30) Spohr, E.; Heinzinger, K. *J. Chem. Phys.* **1986**, *84*, 2304.

(31) Spohr, E.; Heinzinger, K. *Chem. Phys. Lett.* **1986**, *123*, 218.

(32) Linse, P. *J. Chem. Phys.* **1989**, *90*, 4992.

(33) Benjamin, I. *Chem. Rev.* **1996**, *96*, 1449.

(34) Nandi, N.; Bagchi, B. *J. Phys. Chem. B* **1997**, *101*, 10954.

(35) Kohlmeyer, A.; Hartnig, C.; Spohr, E. *J. Mol. Liq.* **1998**, *78*, 233.

(36) Rocchi, C.; Bizzarri, A. R.; Cannistraro, S. *Phys. Rev. E* **1998**, *57*, 3315.

(37) Safran, S. A. *Statistical Mechanics of Surfaces, Interfaces, and Membranes*; Addison-Wesley: Reading, MA, 1994.

(38) Borkovec, M. *J. Chem. Phys.* **1989**, *91*, 6268.

(39) Ennis, J. *J. Chem. Phys.* **1992**, *97*, 663.

(40) Mitchell, D. J.; Ninham, B. W. *J. Chem. Soc., Faraday Trans. 2* **1981**, *77*, 601.

(41) Eicke, H.-F.; Rehak, J. *Helv. Chim. Acta* **1976**, *59*, 2883.

(42) Day, R. A.; Robinson, B. H.; Clarke, J. H. R.; Doherty, J. V. *J. Chem. Soc., Faraday Trans. 1* **1979**, *75*, 132.

(43) Christopher, D. J.; Yarwood, J.; Belton, P. S.; Hills, B. P. *J. Colloid Interface Sci.* **1992**, *152*, 465.

(44) Onori, G.; Santucci, A. *J. Phys. Chem.* **1993**, *97*, 5430.

(45) D'Angelo, M.; Onori, G.; Santucci, A. *Nuovo Cimento* **1994**, *16*, 1601.

(46) Moran, P. D.; Bowmaker, G. A.; Cooney, R. P.; Bartlett, J. R.; Woolfrey, J. L. *Langmuir* **1995**, *11*, 738.

(47) Temsamani, M. B.; Maeck, M.; El Hassani, I.; Hurwitz, H. D. *J. Phys. Chem. B* **1998**, *102*, 3335.

(48) Hauser, H.; Haering, G.; Pande, A.; Luisi, P. L. *J. Phys. Chem.* **1989**, *93*, 7869.

(49) Carlström, G.; Halle, B. *Langmuir* **1988**, *4*, 1346.

(50) Linse, P.; Halle, B. *Mol. Phys.* **1989**, *67*, 537.

(51) Kenez, P. H.; Carlstrom, G.; Furo, I.; Halle, B. *J. Phys. Chem.* **1992**, *96*, 9524.

(52) El Seoud, O. A. *J. Mol. Liq.* **1997**, *72*, 85.

(53) Belletête, M.; Lachapelle, M.; Durocher, G. *J. Phys. Chem.* **1990**, *94*, 7642.

(54) Zhang, J.; Bright, F. V. *J. Phys. Chem.* **1991**, *95*, 7900.

(55) Cho, C. H.; Chung, M.; Lee, J.; Nguyen, T.; Singh, S.; Vedamuthu, M.; Yao, S. H.; Zhu, J. B.; Robinson, G. W. *J. Phys. Chem.* **1995**, *99*, 7806.

(56) Sarkar, N.; Das, K.; Datta, A.; Das, S.; Bhattacharyya, K. *J. Phys. Chem.* **1996**, *100*, 10523.

(57) Datta, A.; Mandal, D.; Pal, S. K.; Bhattacharyya, K. *J. Phys. Chem. B* **1997**, *101*, 10221.

(58) Riter, R. E.; Kimmel, J. R.; Undiks, E. P.; Levinger, N. E. *J. Phys. Chem. B* **1997**, *101*, 8292.

(59) Riter, R. E.; Willard, D. M.; Levinger, N. E. *J. Phys. Chem. B* **1998**, *102*, 2705.

(60) Riter, R. E.; Undiks, E. P.; Levinger, N. E. *J. Am. Chem. Soc.* **1998**, *120*, 6062.

(61) Kim, J.; Lee, M. *J. Phys. Chem. A* **1999**, *103*, 3378.

(62) D'Aprano, A.; Lizzio, A.; Liveri, V. T. *J. Phys. Chem.* **1987**, *91*, 4749.

(63) Shen, X.; Gao, H.; Wang, X. *Phys. Chem. Chem. Phys.* **1999**, *1*, 463.

(64) Dvolaitzky, M.; Guyot, M.; Lagües, M.; Pesant, J. P. L.; Ober, R.; Sauterey, C.; Taupin, C. *J. Chem. Phys.* **1978**, *69*, 3279.

(65) Crupi, V.; Magazu, S.; Maisano, G.; Majolino, D.; Migliardo, P. *Phys. Scr.* **1994**, *50*, 200.

(66) Herwig, K. W.; Dozier, W. D.; Huang, J. S. In *Materials Research Using Cold Neutrons at Pulsed Neutron Sources*; Thiyagarajan, P., Trouw, F., Marzec, B., Loong, C.-K., Eds.; World Scientific: Singapore, 1999.

(67) Novaki, L. P.; El Seoud, O. A. *J. Colloid Interface Sci.* **1998**, *202*, 391.

(68) Pant, D.; Riter, R. E.; Levinger, N. E. *J. Chem. Phys.* **1998**, *109*, 9995.

(69) Mittleman, D. M.; Nuss, M. C.; Colvin, V. L. *Chem. Phys. Lett.* **1997**, *275*, 332.

(70) Griffiths, J. A.; Heyes, D. M. *Langmuir* **1996**, *12*, 2418.

(71) Tobias, D. J.; Klein, M. L. *J. Phys. Chem.* **1996**, *100*, 6637.

(72) Alaimo, M. H.; Kumosinski, T. F. *Langmuir* **1997**, *13*, 2007.

(73) Derecskei, B.; Derecskei-Kovacs, A.; Schelly, Z. A. *Langmuir* **1999**, *15*, 1981.

(74) Brown, D.; Clarke, J. H. R. *J. Phys. Chem.* **1988**, *92*, 2881.

(75) Hill, T. L. *An Introduction to Statistical Thermodynamics*; Dover: New York, 1986; p 144.

(76) Berendsen, H. J. C.; Grigera, J. R.; Straatsma, T. P. *J. Chem. Phys.* **1987**, *91*, 6269.

(77) Reddy, M. R.; Berkowitz, M. *Chem. Phys. Lett.* **1989**, *155*, 173.

(78) Smith, P. E.; van Gunsteren, W. F. *Chem. Phys. Lett.* **1993**, *215*, 315.

(79) Svishchev, I. M.; Kusalik, P. G. *J. Phys. Chem.* **1994**, *93*, 728.

(80) Koneshan, S.; Rasaiah, J. C.; Lynden-Bell, R. M.; Lee, S. H. *J. Phys. Chem. B* **1998**, *102*, 4193.

(81) Schweighofer, K. J.; Essmann, U.; Berkowitz, M. *J. Phys. Chem. B* **1997**, *101*, 3793.

(82) Kohlmeyer, A.; Witschel, W.; Spohr, E. *Chem. Phys.* **1996**, *213*, 211.

(83) Ciccotti, G.; Ryckaert, J.-P. *Comput. Phys. Rep.* **1986**, *4*, 345.

(84) Allen, M. P.; Tildesley, D. J. *Computer Simulation of Liquids*; Clarendon: Oxford, U.K., 1987.

(85) Berendsen, H. J. C.; Postma, J. P. M.; van Gunsteren, W. F.; DiNola, A.; Haak, J. R. *J. Chem. Phys.* **1984**, *81*, 3684.

(86) Eicke, H.-F.; Kvita, P. In *Reverse Micelles*; Luisi, P. L., Straub, B. E., Eds.; Plenum: New York, 1984; pp 21−36.

(87) Zhang, L.; Davis, H. T.; Kroll, D. M.; White, H. S. *J. Phys. Chem.* **1995**, *99*, 2878.

(88) Böttcher, C. J. F. *Theory of Electric Polarization*, 2nd ed.; Elsevier: Amsterdam, 1973; Vol. 1.

(89) Hartnig, C.; Witschel, W.; Spohr, E. *J. Phys. Chem. B* **1998**, *102*, 1241.

(90) Faeder, J.; Ladanyi, B. M., to be submitted.

(91) Sonnenschein, R.; Heinzinger, K. *Chem. Phys. Lett.* **1983**, *102*, 550.

(92) Valleau, J. P.; Gardner, A. A. *J. Chem. Phys.* **1987**, *86*, 4162.

(93) Spohr, E. *J. Chem. Phys.* **1997**, *106*, 388.

(94) Gardner, A. A.; Valleau, J. P. *J. Chem. Phys.* **1987**, *86*, 4171.

(95) Rovere, M.; Ricci, M. A.; Vellati, D.; Bruni, F. *J. Chem. Phys.* **1998**, *108*, 9859.

(96) Spohr, E.; Hartnig, C.; Gallo, P.; Rovere, M. *J. Mol. Liq.* **1999**, *80*, 165.

(97) Schweighofer, K. J.; Essmann, U.; Berkowitz, M. *J. Phys. Chem. B* **1997**, *101*, 10775.

(98) Grigolini, P.; Maestro, M. *Chem. Phys. Lett.* **1986**, *127*, 248.

(99) Giammona, G.; Goffredi, F.; Turco Liveri, V.; Vassallo, G. *J. Colloid Interface Sci.* **1992**, *154*, 411.

(100) Palmer, B. J.; Liu, J. *Langmuir* **1996**, *12*, 746.